

Article

Stability Study of Multi-Level Grayscale Based on Driving Waveforms for Electrowetting Displays

Wanzhen Xu ^{1,2}, Zichuan Yi ^{1,*} , Zhengxing Long ^{1,3}, Hu Zhang ¹, Jiaquan Jiang ¹, Liming Liu ¹, Feng Chi ¹, Ding Tan ⁴ and Huan Wang ⁵

¹ College of Electronic Information, University of Electronic Science and Technology of China, Zhongshan Institute, Zhongshan 528402, China; 2021024102@m.scnu.edu.cn (W.X.); mikaellzx@163.com (Z.L.); 202021020727@std.uestc.edu.cn (H.Z.); m15820735404@163.com (J.J.); liulmxps@126.com (L.L.); chifeng@semi.ac.cn (F.C.)

² South China Academy of Advanced Optoelectronics, South China Normal University, Guangzhou 510006, China

³ School of Information and Optoelectronic Science and Engineering, South China Normal University, Guangzhou 510006, China

⁴ Power China Hubei Engineering Co., Ltd., Wuhan 430048, China; td-hb@powerchina.cn

⁵ Hydro Electric Power System Engineering Company, Wuhan 430000, China; wanghuan3-js@powerchina-hb.com

* Correspondence: yizichuan@zsc.edu.cn; Tel.: +86-173-2282-6330

Abstract: Electrowetting Display (EWD) is a new reflective display with an outstanding performance of color video playback. However, some problems still exist and affect its performance. For instance, oil backflow, oil splitting, and charge trapping phenomena may occur during the driving process of EWDs, which would decrease its stability of multi-level grayscales. Therefore, an efficient driving waveform was proposed to solve these disadvantages. It consisted of a driving stage and a stabilizing stage. First, an exponential function waveform was used in the driving stage for driving the EWDs quickly. Then, an alternating current (AC) pulse signal waveform was used in the stabilizing stage to release the trapped positive charges of the insulating layer to improve display stability. A set of four level grayscale driving waveforms were designed by using the proposed method, and it was used in comparative experiments. The experiments showed that the proposed driving waveform could mitigate oil backflow and splitting effects. Compared to a traditional driving waveform, the luminance stability was increased by 8.9%, 5.9%, 10.9%, and 11.6% for the four level grayscales after 12 s, respectively.

Keywords: electrowetting; multi-level grayscales; driving waveform; oil backflow



Citation: Xu, W.; Yi, Z.; Long, Z.; Zhang, H.; Jiang, J.; Liu, L.; Chi, F.; Tan, D.; Wang, H. Stability Study of Multi-Level Grayscale Based on Driving Waveforms for Electrowetting Displays. *Micromachines* **2023**, *14*, 1123. <https://doi.org/10.3390/mi14061123>

Academic Editor: Aiqun Liu

Received: 12 May 2023

Revised: 24 May 2023

Accepted: 25 May 2023

Published: 26 May 2023



Copyright: © 2023 by the authors. Licensee MDPI, Basel, Switzerland. This article is an open access article distributed under the terms and conditions of the Creative Commons Attribution (CC BY) license (<https://creativecommons.org/licenses/by/4.0/>).

1. Introduction

With the continuous progress of science and technology, display technology has developed rapidly, including EWDs [1–5]. As a new type of display device based on electrowetting (EW) technology, EWDs are widely used in wearable electronic devices, electronic tags, and other fields due to their low power consumption, wide viewing angle, and excellent readability in sunlight [6–8]. Therefore, EWDs have a high development value and broad development prospects [9].

EW technology was proposed by G. Beni as early as 1981 [10]. In 2003, Hayes prepared an EWD based on pixels [11,12]. The performance of EWDs introduced in 2004 went even further; the luminance of the EWDs was four times that of conventional reflective liquid crystal displays (LCDs) [13]. In 2011, a method of filling different colored oil into sub-pixels was achieved for realizing a single-layer, multi-color EWD [14]. Despite tremendous progress in the development of EWDs, some defects, such as oil splitting, oil backflow, charge trapping, and hysteresis effect [15–20], have a bad effect on the display quality. Regarding display principles, EWDs can be improved from interface materials, pixel

structures, fluid motion mechanisms, and driving waveforms [21–25]. Many scholars have contributed to improving the performance of EWDs mainly in terms of display principles and driving waveform design, which can be reflected by grayscale stability, and the grayscale stability is affected by oil splitting and oil backflow [26–28]. Oil splitting is mainly caused by a sudden change in the driving voltage [29,30]. Therefore, a linear function waveform and an exponential function waveform were proposed to solve this problem [31,32]. Oil backflow is a phenomenon of decreasing aperture ratio caused by charge trapping, which can trap charges in an insulating layer of the EWDs [33]. In order to resolve oil backflow, a driving waveform with a reset signal was proposed for releasing captured charges [34]. These excellent driving waveforms provided inspiration and precious experience for driving waveform design. However, EWDs still do not obtain good stability at multi-level grayscales.

In this paper, based on the analysis of the driving principle, a combined driving waveform was proposed to improve the stability of multi-level grayscales. An exponential function waveform was used to decrease sudden changes in the driving voltage, which can prevent oil splitting. According to charge trapping theory, an AC pulse signal waveform can be used to release trapped charges, which can improve the stability of EWDs.

2. Driving Principle of EWDs

Principle of EWDs

EW technology means that the wettability of droplets on a substrate can be changed by applying a voltage [35–37]. Based on the EW principle, the EWD structure can be designed, whose main component is pixels; each pixel consists of a substrate, a pixel electrode, an insulating layer, a pixel wall, colored oil, NaCl solution, a common electrode, and a top plate [2,38–41]. Its structure is shown in Figure 1.

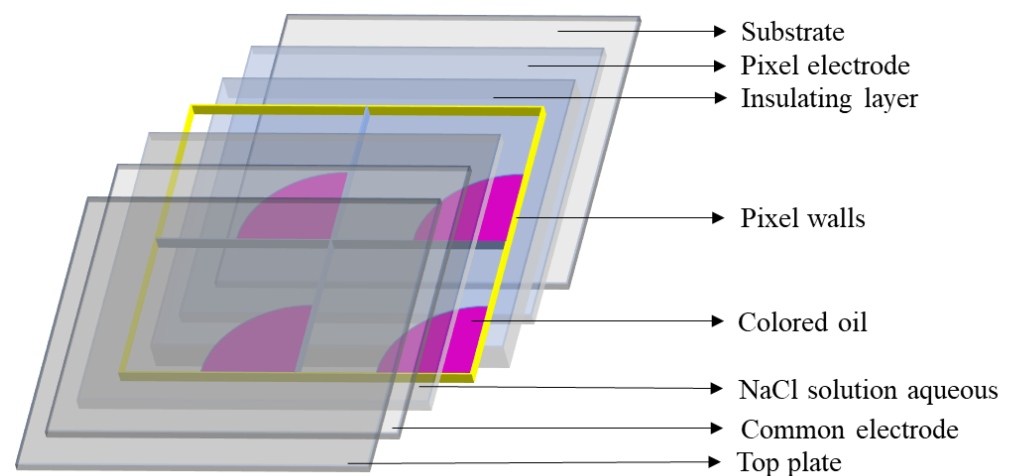


Figure 1. A three-dimensional schematic diagram of pixels in EWDs. It is composed of a substrate, a pixel electrode, an insulating layer, pixel wall, colored oil, NaCl aqueous solution, and a common electrode.

In terms of EWD parameters, the threshold voltage, contact angle, and aperture ratio are used to explain the driving process. The threshold voltage of EWDs is the minimum voltage at which the luminance begins to change during the driving process. When a voltage applied between two electrodes is less than the threshold voltage, the insulating layer appears hydrophobic, and colored oil is laid flat in the pixel, as shown in Figure 2. The original equilibrium state of the system is broken, and the solid–liquid contact angle gradually decreases when the voltage between the two electrodes gradually increases. The wettability of the insulating layer is changed, and it appears oleophobic. Thus, the colored oil is pushed to a corner of the pixel by the NaCl aqueous solution, as shown in Figure 3. The contact area between the shrinking oil and the hydrophobic insulating layer is gradually decreased, and eventually, the entire system can reach a new equilibrium state. When the colored oil is pushed away, the ratio of the uncovered area of the colored

oil to the area of the pixel is called the aperture ratio, which reflects the luminance of EWDs. The contact angle is another critical parameter in measuring the performance of EWDs, which is a tangency angle at the intersection of solid, liquid, and gas phases. The famous Lippmann–Young Equation derived in 1875 can be used to describe the relationship between the contact angle and applied voltage [42], as shown in Equation (1).

$$\cos \theta_V - \cos \theta_0 = KV^2 \quad (1)$$

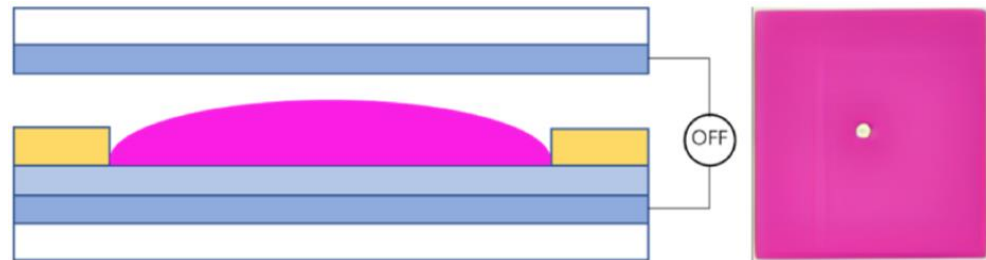


Figure 2. A two-dimensional structure diagram and planform of a pixel in an EWD when no voltage is applied.

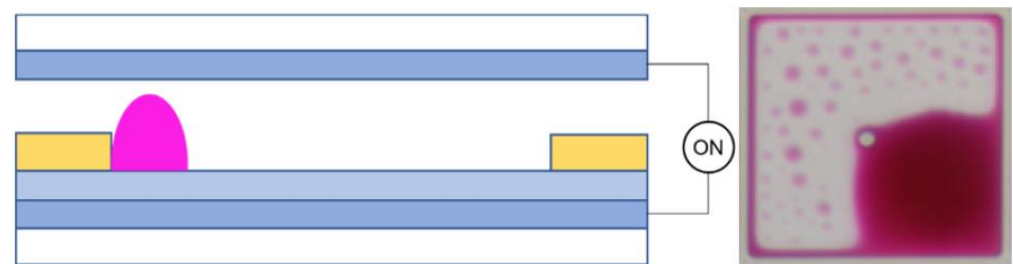


Figure 3. A two-dimensional structure diagram and planform of a pixel in an EWD when a voltage is applied.

θ_0 and θ_V are the contact angles before and after the application of a driving voltage, respectively, and K is a constant related to the material and structure of the EWDs. Ideally, the square of the driving voltage is proportional to the contact angle. However, due to factors such as oil backflow and charge trapping, the Equation (1) can be optimized as Equation (2); V_G is the voltage generated by the charge trapping.

$$\cos \theta_V - \cos \theta_0 = K(V - V_G)^2 \quad (2)$$

3. Experimental Results and Discussion

3.1. Experimental Platform

In this experiment, an integrated experiment platform was built to measure and record luminance and response time values, which consisted of a computer, a function generator, a voltage amplifier, a colorimeter, and a microscope. The entire system could be operated as follows. First, driving waveforms were designed on the computer by using professional software (Matlab R2019a). A binary file would be generated, which would describe driving waveforms, and then the file would be stored in the function generator. Due to the limited output voltage of the function generator, the voltage amplifier was used to amplify the driving waveform for driving the EWDs. During the driving process, the colorimeter was applied to measure and record the luminance of the EWDs, and the microscope was used to observe the colored oil in the pixels. The parameters of the instruments used above are shown in Table 1, and the whole experiment platform is shown in Figure 4.

Table 1. Parameters of the experimental instruments.

Name	Model	Manufacturers	Region	Region
Computer	H430	Lenovo	Beijing	China
Function generator	AFG3022C	Tektronix	Beaverton	USA
Voltage amplifier	ATA-2022H	Agitek	Xian	China
Microscope	SZ680	Cnoptec	Chongqing	China
Colorimeter	Arges-45	Admesy	Ittervoort	Netherlands

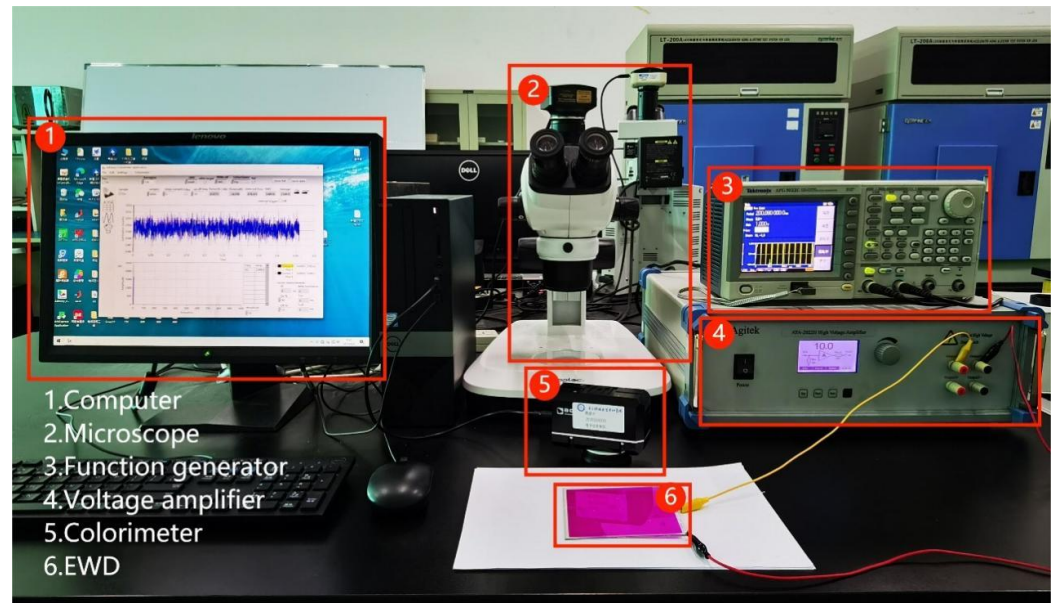


Figure 4. The experimental platform for evaluating the performance of EWDs. It was composed of a computer, a microscope, a function generator, a voltage amplifier, a colorimeter, and an EWD. The EWD was the testing object. The computer was used to design the waveforms. The microscope was used to observe the microscopic forms of the EWD. The function generator and voltage amplifier were used to generate the driving waveforms. The colorimeter was used to measure the luminance of the EWD.

In the experiment, the EWD used for testing was designed and manufactured by us, as shown in Figure 5. The parameters of the EWD are shown in Table 2.

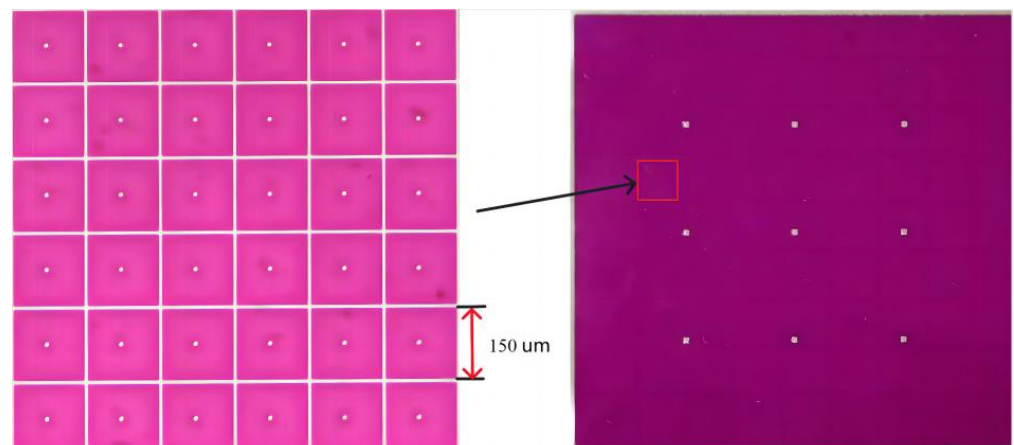


Figure 5. The EWD used for evaluating the display performance.

Table 2. Parameters of the EWD panel.

Panel Size	Oil Color	Resolution	Pixel Size	Pixel Wall Height	Insulating Layer Thickness	Electrode Plates Thickness
10 × 10 cm	magenta	320 × 240	150 × 150 μm	18 μm	1 nm	2.5 nm

3.2. Proposed Driving Waveforms

In order to drive the EWDs to realize maximum luminance and stable performance at a specific grayscale, a driving waveform based on an exponential function and an AC square wave was proposed, including a driving stage and a stabilizing stage, as shown in Figure 6.

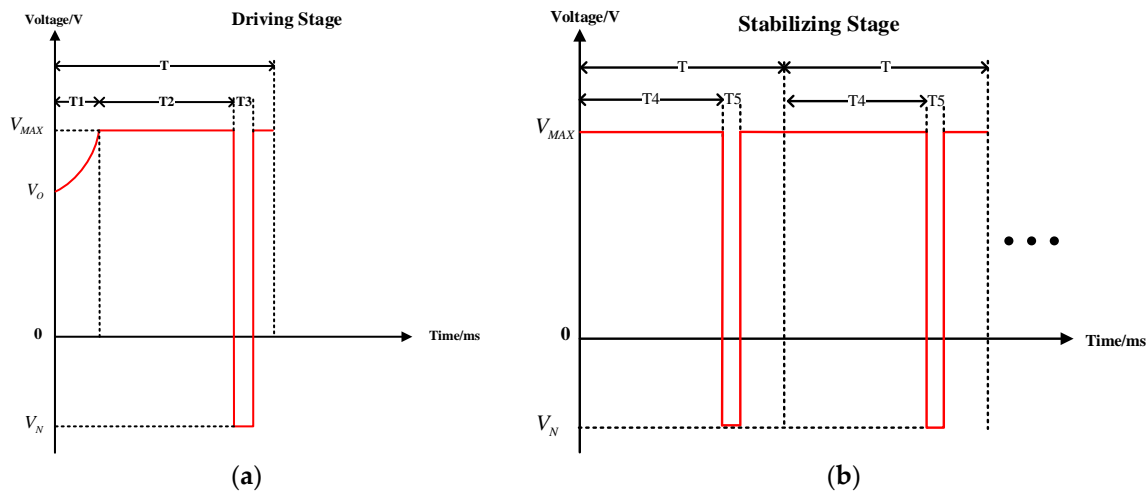


Figure 6. Schematic diagrams of the proposed driving waveform. (a) The diagram of the driving stage. V_{MAX} was a voltage at which the pixel could be driven to the target grayscale, and it was also called a target driving voltage. V_N was a negative voltage, which could release trapped charges. V_0 was an initial rising voltage. T was the duration of a display cycle. T_1 was the duration of the exponential function waveform. T_2 was the duration of the DC driving process. T_3 was the duration of the negative voltage in the driving stage. (b) The diagram of the stabilizing stage. T_4 was the duration of the DC driving process in the stabilizing stage. T_5 was the duration of the negative voltage in the stabilizing stage.

In the driving stage, the proposed waveform was mainly based on an exponential function and an AC square. The exponential function was used to drive the EWDs to achieve maximum luminance quickly. The AC square was used to release trapped charges, which can reduce the effect of V_G in Equation (2) and suppress oil backflow in the driving stage. The equation of the exponential function is shown in Equation (3).

$$U = (V_0 - 1) + e^{at} \tag{3}$$

U is the driving voltage in real-time. a is a time constant. V_0 is the initial voltage. It could be observed that a affected the rising rate of the driving voltage. Therefore, T_1 could keep a constant by adjusting a when the target driving voltage was different. In the stabilizing stage, the proposed driving waveform was composed of many display cycles. Each display cycle had an AC square, which was used to keep the EWD's display stable.

3.3. Parameter Optimization of the Driving Stage

In the driving stage, parameters would be optimized according to the relationship between the luminance and the driving voltage. Therefore, to obtain the relationship, a DC waveform was designed, which was set to 0 V to 25 V, and the maximum voltage was set to 25 V to protect the EWDs. Figure 7 shows the corresponding relationship between the

DC driving voltage and the luminance. The luminance showed an upward trend, and the growth rate decreased gradually. The EWD could not be driven when the positive voltage was lower than 7 V. The EWD also could not be driven when the negative voltage was lower than 4 V. Therefore, the positive and negative threshold voltage amplitude were set to 7 and 4 V, respectively.

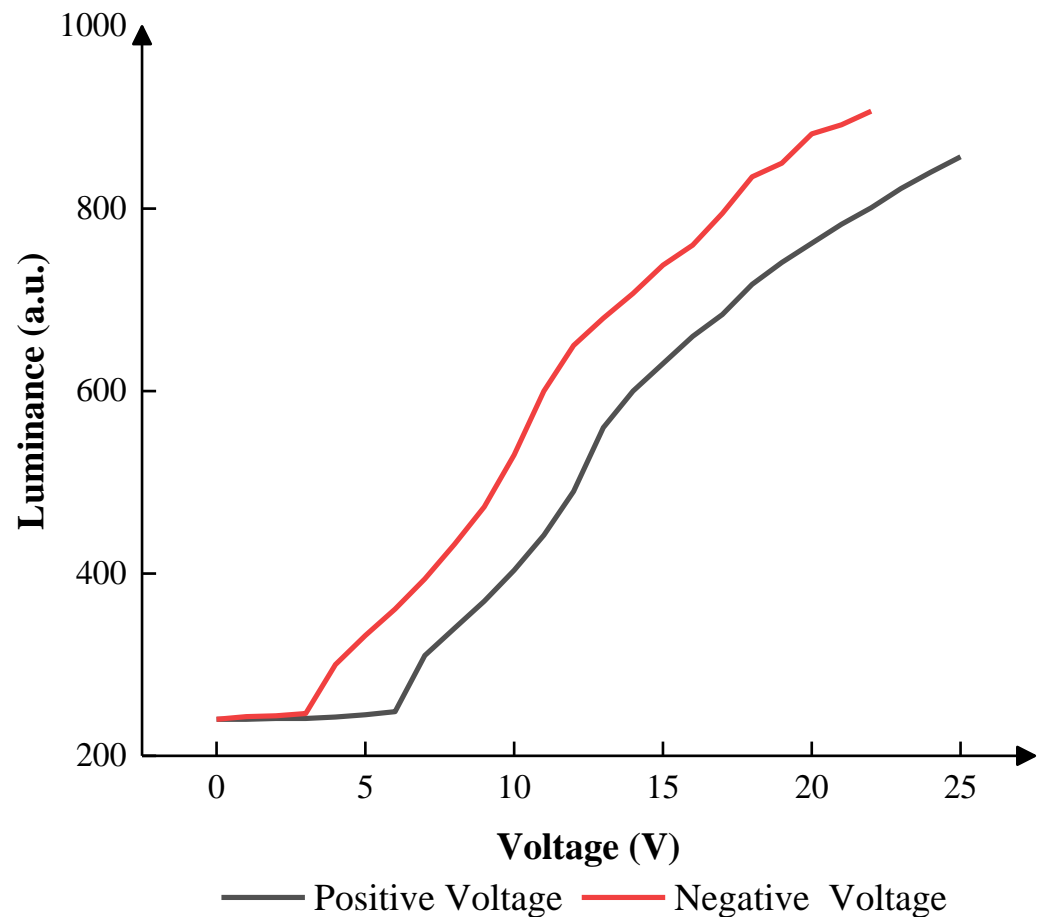


Figure 7. The luminance of the EWD, which was applied to different DC voltages. The luminance was 240 when the positive DC voltage was less than 7 V. The luminance was 243 when the negative DC voltage was less than 4 V. The maximum luminance was obtained when the DC voltage was 25 V.

According to Figure 7, the maximum luminance was 857 when 25 V-positive DC voltage was applied. In this paper, the number of grayscales was set to four as an illustrative example, and the luminance of four grayscales was set to 400, 500, 600, and 700. The target driving voltages were set to 10 V, 12 V, 14 V, and 18 V, and the luminance values were 403, 490, 600, and 717, respectively. The display cycle T was set to 20 ms because 50 Hz was a usual frequency that could not be recognized by eyes. V_N was used to release trapped charges. T_1 was set to 5 ms. T_2 was set to 13 ms to drive the EWD at the maximum luminance. T_3 was set to 0.25 ms to release trapped charges, which could prevent oil backflow caused by charge trapping. According to Equation (3), V_0 was set to 7 V, 9 V, 11 V, and 14 V to obtain driving waveforms of the same shape in four grayscales when T_1 was 5 ms. The range of V_N was set to 4–10 V, 6–12 V, 8–14 V, and 12–18 V. The luminance between different grayscales and V_N in 200 ms is shown in Figure 8.

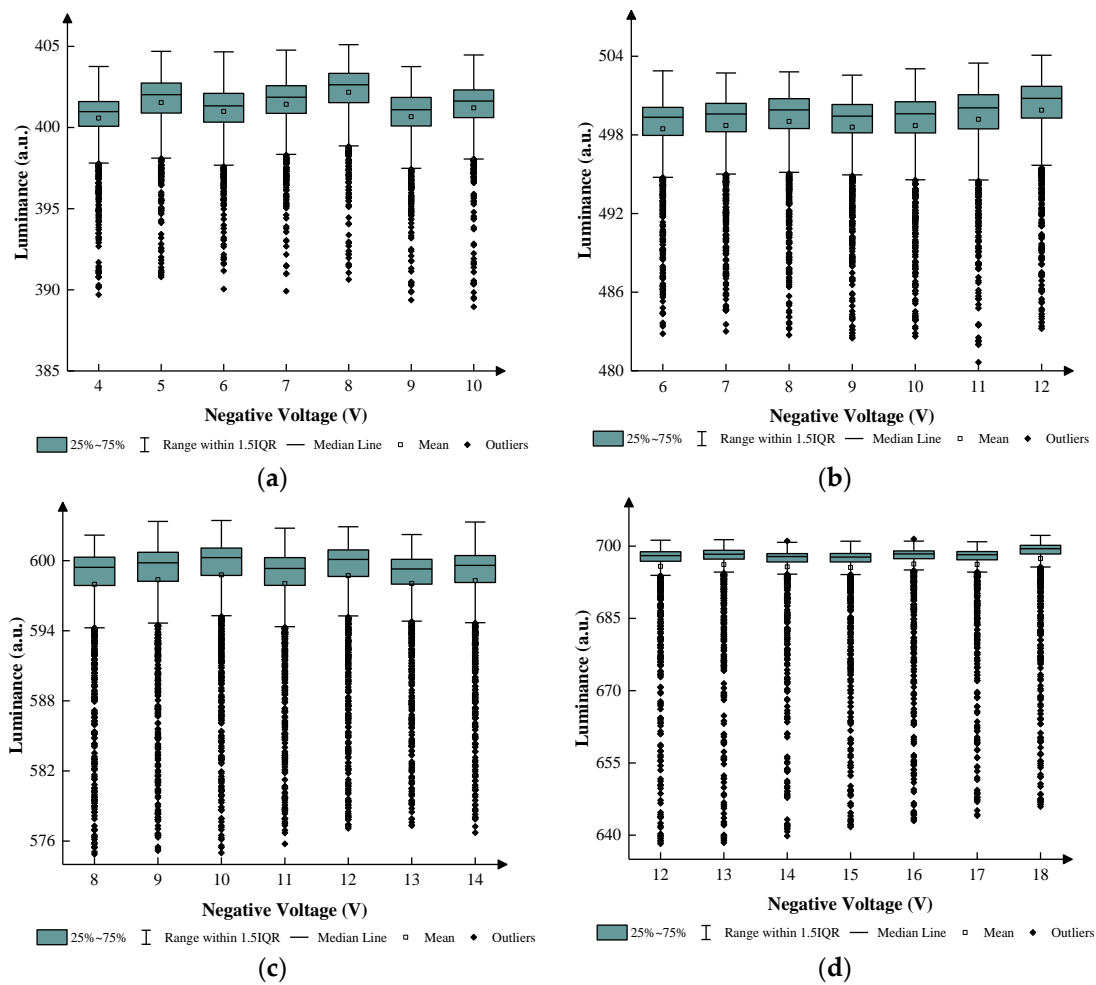


Figure 8. The luminance of the EWD when different negative voltages were applied. The median line, mean, and other parameters reflect the distribution of the luminance. (a) Relationship between luminance values and negative voltages at the first grayscale. (b) Relationship between luminance values and negative voltages at the second grayscale. (c) Relationship between luminance values and negative voltages at the third grayscale. (d) Relationship between luminance values and negative voltages at the fourth grayscale.

According to Figure 8, the luminance of the EWD barely changed when V_N was lower than V_{MAX} . In the first grayscale, the median luminance was maintained at approximately 402 when V_N was set to 4–10 V. The average luminance was slightly less than the median luminance but remained above 400. The interquartile range (IQR) was maintained at approximately 3. The difference between the burr signal and the stable luminance was within 12. In the second grayscale, the median luminance was maintained at approximately 500 when V_N was set to 6–12 V. The average luminance was slightly less than the median luminance, but it was very close to 500. The IQR was maintained at approximately 3. The difference between the burr signal and the stable luminance was within 18. In the third grayscale, the median luminance was maintained at approximately 599 when V_N was set to 8–14 V. The average luminance was slightly less than the median luminance, but it was very close to 598. The IQR was maintained at approximately 4. The difference between the burr signal and the stable luminance was within 25. In the fourth grayscale, the median luminance was maintained at approximately 698 when V_N was set to 12–18 V. The average luminance was slightly less than the median luminance, but it was very close to 694. The IQR was maintained at approximately 3. The difference between the burr signal and the stable luminance was within 62. The applied negative voltage hardly influenced the

luminance. Therefore, V_{NS} were set to 4 V, 6 V, 8 V, and 12 V in different grayscales. Figure 9 demonstrates the relationship between the driving time and the luminance of the EWD when negative voltages were set to 4 V, 6 V, 8 V, and 12 V in four grayscales, respectively.

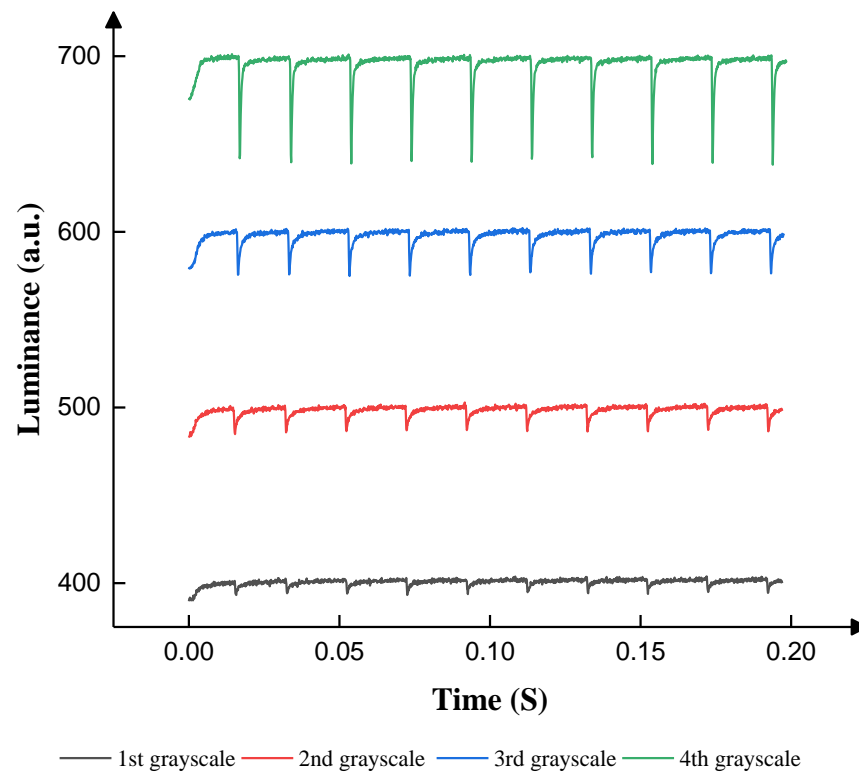


Figure 9. The luminance of the EWD when different amplitude negative voltages were applied.

3.4. Testing of the Stabilizing Stage

In the driving stage, the applied negative voltage was evaluated to obtain the optimum negative voltage. The luminance would decrease when a negative voltage was applied. T_3 was set to 0.25 ms due to the limitation of the display cycle. In the stabilizing stage, only T_4 and T_5 would be considered. T_4 was set to 15 ms to keep a stable luminance. T_5 could be set to 0.1 ms, 0.25 ms, 0.5 ms, 1 ms, and 2 ms in four grayscales, respectively. Negative voltages were set to 4 V, 6 V, 8 V, and 12 V, respectively. Figure 10 shows the relationship between luminance and T_5 in different grayscales within 200 ms.

According to Figure 10, the luminance distribution of the EWD changed when T_5 was changed. As T_5 increased, the luminance fluctuation also increased. In the first grayscale, the median luminance of the EWD maintained at approximately 401 when T_5 was set to 0.1 ms, 0.25 ms, 1 ms, and 2 ms. The average luminance declined below 400 when T_5 was set to 1 and 2 ms. The IQR increased from 2 to 10 when T_5 increased; therefore, the display stability became worse. The EWD had better stability within 200 ms when T_5 was lower than 2 ms. In the second grayscale, the median luminance and average luminance maintained at approximately 500 when T_5 was set to 0.1 ms, 0.25 ms, and 0.5 ms. The median luminance and average luminance decreased below 500 when T_5 was set to 1 ms and 2 ms. The IQR increased from 2 to 20 when T_5 increased. The EWD had better stability within 200 ms when T_5 was lower than 2 ms. In the third grayscale, the median luminance and average luminance maintained at approximately 600 when T_5 was set to 0.1 ms, 0.25 ms, and 0.5 ms. The median luminance and average luminance decreased below 600. The IQR increased from 2 to 20 when T_5 increased. The EWD had better stability within 200 ms when T_5 was smaller than 1 ms. In the fourth grayscale, the median luminance and average luminance maintained at approximately 700 when T_5 was set to 0.1 and 0.25 ms. The median luminance and average luminance increased over 600 when T_5 was set to 0.5 ms, 1 ms, and 2 ms. The

IQR increased from 2 to 10 when T_5 increased. Therefore, the EWD had better stability within 200 ms when T_5 was set to 0.1 ms, 0.25 ms, and 0.5 ms in four grayscales.

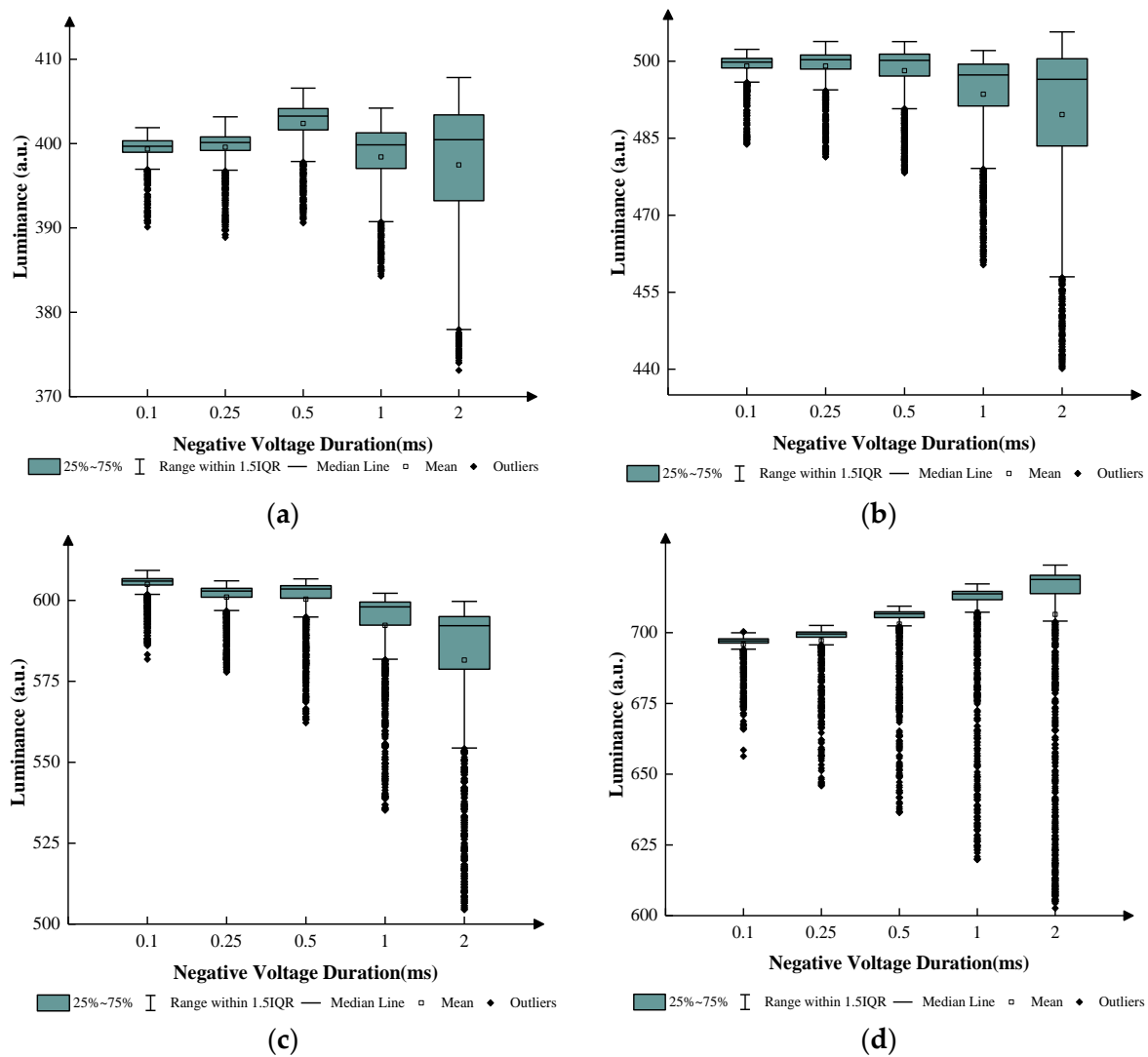


Figure 10. The luminance of the EWD within 200 ms when negative voltages were applied. The median line, mean, and other parameters reflect the distribution of the luminance. (a) Relationship between luminance values and negative voltages at the first grayscale. (b) Relationship between luminance values and negative voltages at the second grayscale. (c) Relationship between luminance values and negative voltages at the third grayscale. (d) Relationship between luminance values and negative voltages at the fourth grayscale.

The stability of the EWDs could not be completely proven in a short duration. The relationship between driving time and voltage in a long display duration must be considered in terms of practicality. Due to the charge trapping effect, the insulating layer of the EWD stored charges continuously when a unipolar voltage was applied for a long duration, which caused oil backflow and affected the display performance. Therefore, the negative voltage was designed to suppress the oil backflow. Figure 11 demonstrates the relationship between the driving time and the luminance of the EWDs for a long duration when the negative voltage was set to 4 V, 6 V, 8 V, and 12 V in four grayscales, respectively.

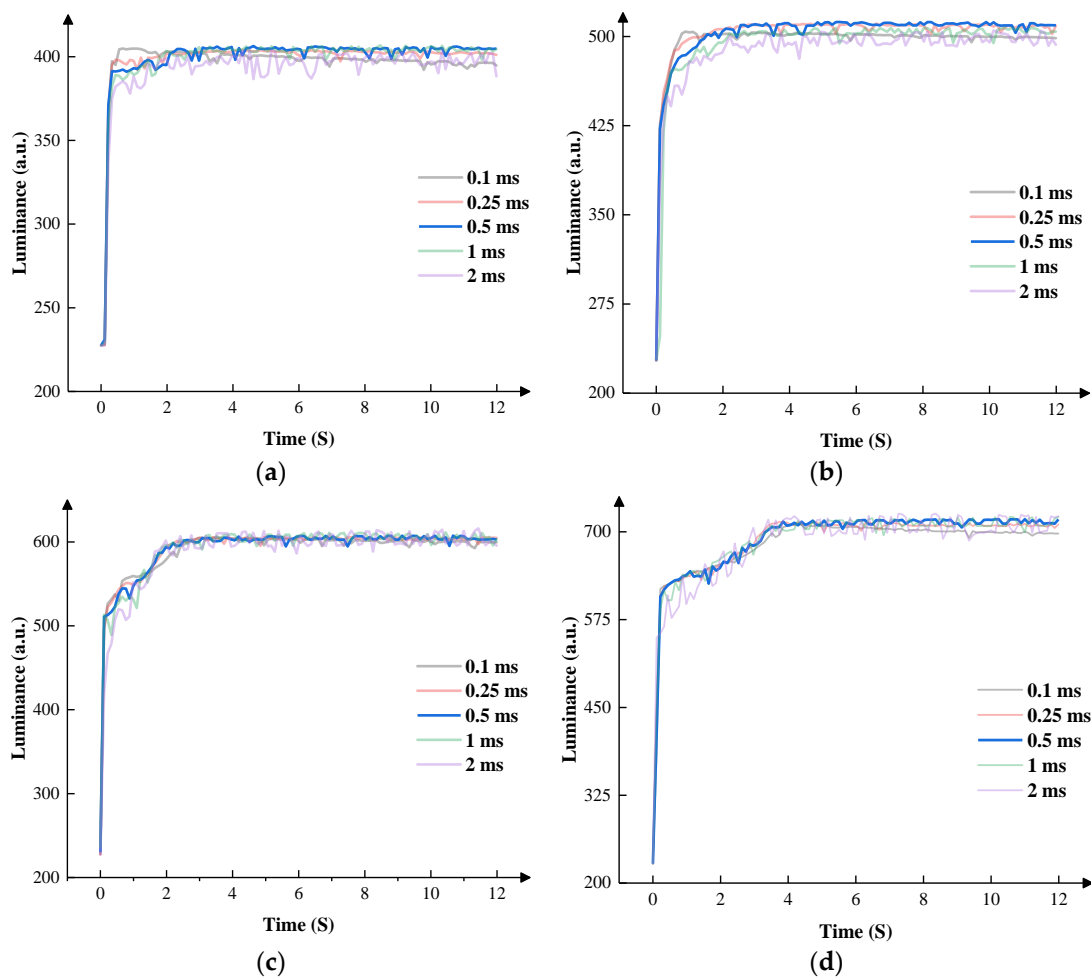


Figure 11. The luminance of the EWDs during a long duration when different negative voltages were applied. (a) Relationship between luminance values and the negative voltage at the first grayscale. (b) Relationship between luminance values and the negative voltage at the second grayscale. (c) Relationship between luminance values and the negative voltage at the third grayscale. (d) Relationship between luminance values and the negative voltage at the fourth grayscale.

According to Figure 11, T_5 was an essential part of the EWD's stability. In the first grayscale, the EWDs obtained the shortest response time when T_5 was set to 0.1 ms. Oil backflow occurred when T_5 was set to 0.1 ms and 0.25 ms, which affected the display stability. Therefore, the EWD could display steadily when T_5 was set to 0.5 ms and 1 ms. Compared to 1 ms, the EWD could obtain a higher luminance and a higher response speed when T_5 was set to 0.5 ms. In the second grayscale, the EWD obtained the shortest response time when T_5 was set to 0.1 ms. Oil backflow occurred when T_5 was set to 0.1 ms. Therefore, the EWDs displayed steadily when T_5 was set to 0.25 ms and 0.5 ms. Compared to 0.25 ms, the EWDs could obtain a higher luminance when T_5 was set to 0.5 ms. In the third grayscale, the EWDs obtained the shortest response time when T_5 was set to 2 ms and obtained the longest response time when T_5 was set to 0.1 ms. Oil backflow occurred when T_5 was set to 0.1 ms. Therefore, the EWDs displayed steadily when T_5 was set to 0.5 and 1 ms. Compared to 0.25 ms, the EWDs could obtain a higher luminance and better stability when T_5 was set to 0.5 ms. In the fourth grayscale, the EWD obtained the shortest response time when T_5 was set to 2 ms. Oil backflow occurred when T_5 was set to 0.1 ms and 0.25 ms. Therefore, the EWDs displayed steadily when T_5 was set to 0.5 and 1 ms. Compared to 1 ms, the EWDs could obtain a higher luminance and a shorter response time when T_5 was set to 0.5 ms. According to Figure 12, the response time of the EWD increased gradually as the grayscale increased.

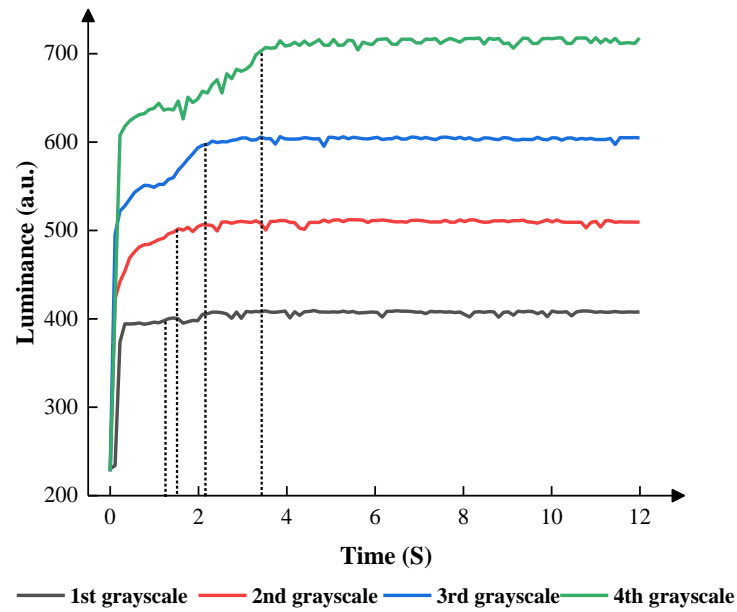


Figure 12. The luminance of the EWDs within a long duration when the best parameters were applied. In the first grayscale, V_N was set to 4 V, and T_5 was set to 0.5 ms. In the second grayscale, V_N was set to 6 V, and T_5 was set to 0.5 ms. In the third grayscale, V_N was set to 8 V, and T_5 was set to 0.5 ms. In the fourth grayscale, V_N was set to 12 V, and T_5 was set to 0.5 ms.

3.5. Performance of the Proposed Waveform

As shown in Figure 13, traditional driving waveforms were used to compare performance with the proposed driving waveform. The rising duration of the driving stage was set to 5 ms, and the target driving voltage V_{MAX} was set to 10 V, 12 V, 14 V, and 18 V. The initial voltage was set to 0 V.

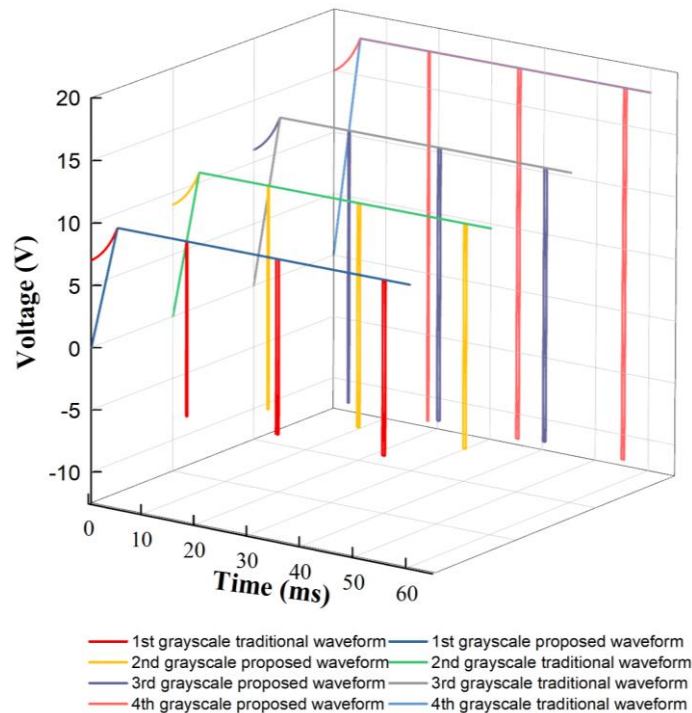


Figure 13. Proposed driving waveforms and traditional driving waveforms of different grayscales for performance comparison.

As shown in Figure 13, traditional driving waveforms were used to compare display performance with the proposed driving waveform. The rising duration of the driving stage was also set to 5 ms, and the target driving voltages were set to 10 V, 12 V, 14 V, and 18 V in four grayscales. The initial voltage was set to 0 V.

According to Figure 14, compared to the traditional driving waveform, the proposed driving waveform had a better performance. In the first grayscale, the luminance of the proposed driving waveform steadily increased to approximately 400 and maintained at 400. Although the traditional driving waveform had a shorter response time, the luminance started to decline after reaching 400. In the second grayscale, the luminance of the proposed driving waveform steadily increased to approximately 500 and was maintained at 510. The luminance of the traditional driving waveform started to decline after reaching 520. In the third grayscale, the luminance of the proposed driving waveform steadily increased to approximately 600 and maintained at 600. The luminance of the traditional driving waveform started to decline after reaching 600. In the fourth grayscale, the luminance of the proposed driving waveform steadily increased to approximately 700 and maintained at 700. The luminance of the traditional driving waveform started to decline after reaching 700. Generally, the proposed driving waveform solved the oil backflow, which was caused by charge trapping. Compared to the traditional driving waveform, the EWD had better stability by applying the proposed driving waveform.

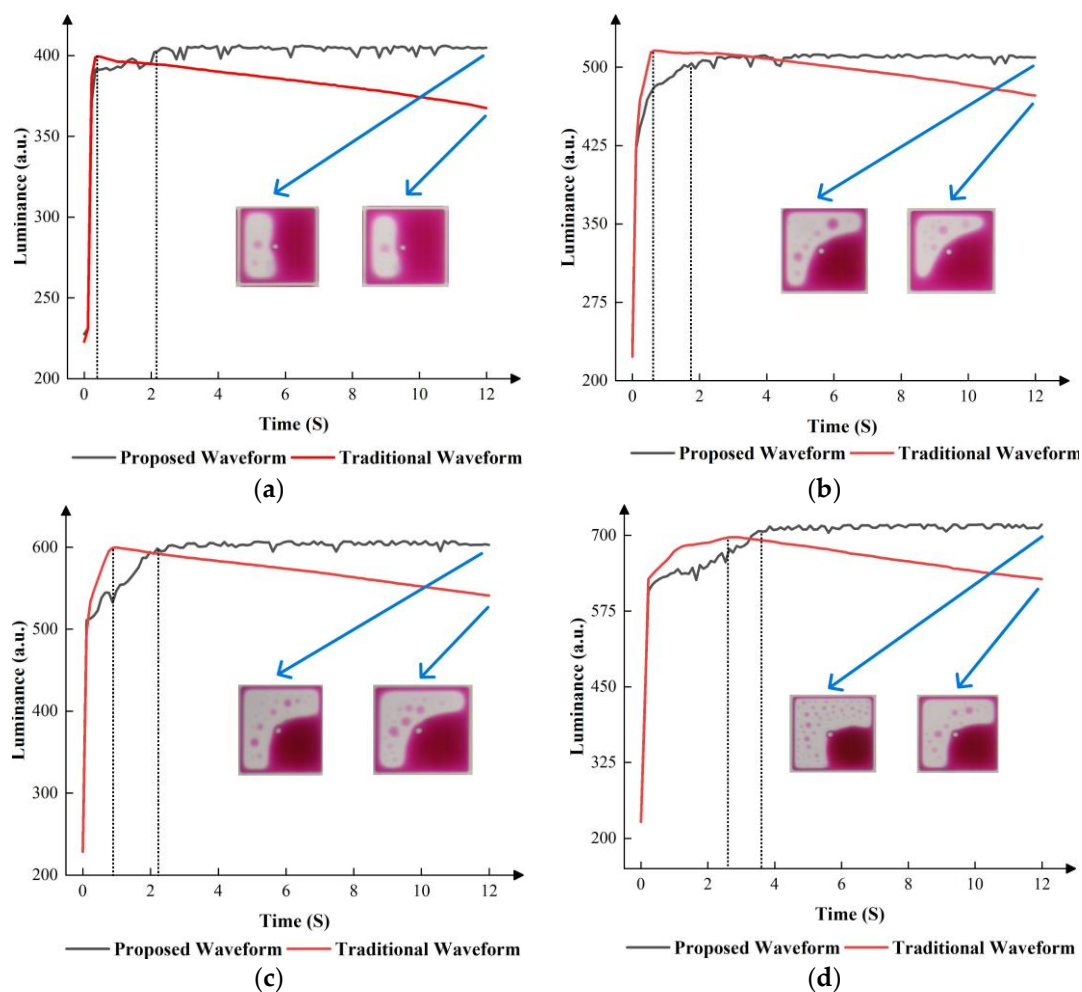


Figure 14. Luminance curves of different driving waveforms in different grayscales. (a) Luminance curves of different driving waveforms in the first grayscale. (b) Luminance curves of different driving waveforms in the second grayscale. (c) Luminance curves of different driving waveforms in the third grayscale. (d) Luminance curves of different driving waveforms in the fourth grayscale.

4. Conclusions

In order to achieve a stable display performance of multi-level grayscales, a new combined driving waveform was proposed in this paper, which was based on an exponential function and AC voltage. Compared to the traditional driving waveform, the effectiveness of the proposed driving waveform was proven. The proposed driving waveform could suppress oil backflow at different grayscales and reduce the luminance oscillation of the EWDs. In addition, the proposed driving waveform could be adapted to drive the EWDs with more than four grayscales. In summary, the proposed driving waveform provided a reference value for improving multi-level display performance of the EWDs.

Author Contributions: W.X. and Z.Y. designed this project. W.X. carried out most of the experiments and data analysis. Z.L., H.Z. and J.J. performed part of the experiments and helped with discussions during manuscript preparation. Z.Y., L.L. and F.C. revised the paper and gave suggestions on project management. D.T. and H.W. provided helpful discussions on the experimental results. All authors have read and agreed to the published version of the manuscript.

Funding: This research was funded by the National Natural Science Foundation of China (no. 62105056), the Innovation Team of Colleges and Universities in Guang-dong Province (no. 2021KCXTD040), the Engineering Technology Research Center of Colleges and Universities in Guang-dong Province (no. 2021GCZX005), and the Construction Project of Professional Quality Engineering in 2020 (no. YLZY202001).

Data Availability Statement: Data is contained within the article.

Conflicts of Interest: The authors declare no conflict of interest.

References

1. You, H.; Steckl, A.J. Three-color electrowetting display device for electronic paper. *Appl. Phys. Lett.* **2010**, *97*, 023514. [[CrossRef](#)]
2. Jin, M.; Shen, S.; Yi, Z.; Zhou, G.; Shui, L. Optofluid-based reflective displays. *Micromachines* **2018**, *9*, 159. [[CrossRef](#)] [[PubMed](#)]
3. Luo, Z.; Fan, J.; Xu, J.; Zhou, G.; Liu, S. A novel driving scheme for oil-splitting suppression in electrowetting display. *Opt. Rev.* **2020**, *27*, 339–345. [[CrossRef](#)]
4. Shui, L.; Hayes, R.A.; Jin, M.; Zhang, X.; Bai, P.; van den Berg, A.; Zhou, G. Microfluidics for electronic paper-like displays. *Lab Chip* **2014**, *14*, 2374–2384. [[CrossRef](#)] [[PubMed](#)]
5. Yi, Z.; Zeng, W.; Ma, S.; Feng, H.; Zeng, W.; Shen, S.; Shui, L.; Zhou, G.; Zhang, C. Design of driving waveform based on a damping oscillation for optimizing red saturation in three-color electrophoretic displays. *Micromachines* **2021**, *12*, 162. [[CrossRef](#)]
6. Luo, Z.; Luo, J.; Zhao, W.; Cao, Y.; Lin, W.; Zhou, G. A high-resolution and intelligent dead pixel detection scheme for an electrowetting display screen. *Opt. Rev.* **2017**, *25*, 18–26. [[CrossRef](#)]
7. Li, W.; Wang, L.; Henzen, A. A multi waveform adaptive driving scheme for reducing hysteresis effect of electrowetting displays. *Front. Phys.* **2020**, *8*, 618811. [[CrossRef](#)]
8. Sureshkumar, P.; Bhattacharyya, S.S. Display applications of electrowetting. *J. Adhes. Sci. Technol.* **2012**, *26*, 1947–1963. [[CrossRef](#)]
9. Yi, Z.; Zhang, H.; Jiang, M.; Wang, J. Editorial for the special issue on advances in optoelectronic devices. *Micromachines* **2023**, *14*, 652. [[CrossRef](#)]
10. Beni, G.; Hackwood, S. Electro-wetting displays. *Appl. Phys. Lett.* **1981**, *38*, 207–209. [[CrossRef](#)]
11. Hayes, R.A.; Feenstra, B.J. Video-speed electronic paper based on electrowetting. *Nature* **2003**, *425*, 383–385. [[CrossRef](#)] [[PubMed](#)]
12. Roques-Carmes, T.; Hayes, R.; Feenstra, B.; Schlangen, L. Liquid behavior inside a reflective display pixel based on electrowetting. *J. Appl. Phys.* **2004**, *95*, 4389–4396. [[CrossRef](#)]
13. Roques-Carmes, T.; Hayes, R.; Schlangen, L. A physical model describing the electro-optic behavior of switchable optical elements based on electrowetting. *J. Appl. Phys.* **2004**, *96*, 6267–6271. [[CrossRef](#)]
14. Ku, Y.; Kuo, S.; Tsai, Y.; Cheng, P.; Chen, J.; Lan, K.; Lo, K.; Lee, K.; Cheng, W. The structure and manufacturing process of large area transparent electrowetting display. *SID Symp. Dig. Tech. Pap.* **2012**, *43*, 850–852. [[CrossRef](#)]
15. Tian, L.; Bai, P. A combined pulse driving waveform with rising gradient for improving the aperture ratio of electrowetting displays. *Front. Phys.* **2021**, *9*, 709151. [[CrossRef](#)]
16. Li, W.; Wang, L.; Zhang, T.; Lai, S.; Liu, L.; He, W.; Zhou, G.; Yi, Z. Driving waveform design with rising gradient and sawtooth wave of electrowetting displays for ultra-low power consumption. *Micromachines* **2020**, *11*, 145. [[CrossRef](#)]
17. Long, Z.; Yi, Z.; Zhang, H.; Liu, L.; Shui, L. Toward suppressing charge trapping based on a combined driving waveform with an ac reset signal for electro-fluidic displays. *Membranes* **2022**, *12*, 1072. [[CrossRef](#)]
18. Chen, Y.; Chiu, Y.; Lee, W.; Liang, C. 56.3: A charge trapping suppression method for quick response electrowetting displays. *SID Symp. Dig. Tech. Pap.* **2010**, *41*, 842–845. [[CrossRef](#)]

19. Gao, J.; Mendel, N.; Dey, R.; Baratian, D.; Mugele, F. Contact angle hysteresis and oil film lubrication in electrowetting with two immiscible liquids. *Appl. Phys. Lett.* **2018**, *112*, 203703. [[CrossRef](#)]
20. Hsieh, W.; Lin, C.; Lo, K.; Lee, K.; Cheng, W.; Chen, K. 3d electrohydrodynamic simulation of electrowetting displays. *J. Micromechanics Microengineering* **2014**, *24*, 125024. [[CrossRef](#)]
21. Yi, Z.; Zhang, H.; Zeng, W.J.; Feng, H.Q.; Long, Z.X.; Liu, L.M.; Hu, Y.F.; Zhou, X.C.; Zhang, C.F. Review of driving waveform for electrowetting displays. *Front. Phys.* **2021**, *9*, 728804. [[CrossRef](#)]
22. Roques-Carnes, T.; Palmier, S.; Hayes, R.A.; Schlangen, L.J.M. The effect of the oil/water interfacial tension on electrowetting driven fluid motion. *Colloids Surf. A Physicochem. Eng. Asp.* **2005**, *267*, 56–63. [[CrossRef](#)]
23. Sureshkumar, P.; Kim, M.; Song, E.; Lim, Y.J.; Lee, S.H. Effect of surface roughness on the fabrication of electrowetting display cells and its electro-optic switching behavior. *Surf. Rev. Lett.* **2009**, *16*, 23–28. [[CrossRef](#)]
24. Yi, Z.; Liu, L.; Wang, L.; Li, W.; Shui, L.; Zhou, G. A driving system for fast and precise gray-scale response based on amplitude-frequency mixed modulation in tft electrowetting displays. *Micromachines* **2019**, *10*, 732. [[CrossRef](#)]
25. Chiu, Y.; Liang, C.; Chen, Y.; Lee, W.; Chen, H.; Wu, S. Accurate-gray-level and quick-response driving methods for high-performance electrowetting displays. *J. Soc. Inf. Disp.* **2011**, *19*, 741–748. [[CrossRef](#)]
26. Yi, Z.; Shui, L.; Wang, L.; Jin, M.; Hayes, R.A.; Zhou, G. A novel driver for active matrix electrowetting displays. *Displays* **2015**, *37*, 86–93. [[CrossRef](#)]
27. Zhang, H.; Yi, Z.; Lv, J.; Liu, L.; Chi, F.; Zhang, C. Improvement of aperture ratio and grayscale stability of electrowetting displays by designing a combined driving waveform of an exponential function and ac voltage. *Displays* **2022**, *74*, 102288. [[CrossRef](#)]
28. Yi, Z.; Feng, W.; Wang, L.; Liu, L.; Lin, Y.; He, W.; Shui, L.; Zhang, C.; Zhang, Z.; Zhou, G. Aperture ratio improvement by optimizing the voltage slope and reverse pulse in the driving waveform for electrowetting displays. *Micromachines* **2019**, *10*, 862. [[CrossRef](#)]
29. Giraldo, A.; Vermeulen, P.; Figura, D.; Spreafico, M.; Meeusen, J.; Hampton, M.; Novoselov, P. Improved oil motion control and hysteresis-free pixel switching of electrowetting displays. *SID Symp. Dig. Tech. Pap.* **2012**, *43*, 625–628. [[CrossRef](#)]
30. He, T.; Jin, M.; Eijkel, J.C.; Zhou, G.; Shui, L. Two-phase microfluidics in electrowetting displays and its effect on optical performance. *Biomicrofluidics* **2016**, *10*, 011908. [[CrossRef](#)]
31. Lu, Y.; Tang, B.; Yang, G.; Guo, Y.; Liu, L.; Henzen, A. Progress in advanced properties of electrowetting displays. *Micromachines* **2021**, *12*, 206. [[CrossRef](#)] [[PubMed](#)]
32. Yi, Z.; Huang, Z.; Lai, S.; He, W.; Wang, L.; Chi, F.; Zhang, C.; Shui, L.; Zhou, G. Driving waveform design of electrowetting displays based on an exponential function for a stable grayscale and a short driving time. *Micromachines* **2020**, *11*, 313. [[CrossRef](#)] [[PubMed](#)]
33. Zhang, T.; Deng, Y. Driving waveform design of electrowetting displays based on a reset signal for suppressing charge trapping effect. *Front. Phys.* **2021**, *9*, 672541. [[CrossRef](#)]
34. Liu, L.; Bai, P.; Yi, Z.; Zhou, G. A separated reset waveform design for suppressing oil backflow in active matrix electrowetting displays. *Micromachines* **2021**, *12*, 491. [[CrossRef](#)]
35. Li, F.; Mugele, F. How to make sticky surfaces slippery: Contact angle hysteresis in electrowetting with alternating voltage. *Appl. Phys. Lett.* **2008**, *92*, 244108. [[CrossRef](#)]
36. Papaderakis, A.; Dryfe, R. The renaissance of electrowetting. *Curr. Opin. Electrochem.* **2023**, *38*, 101245. [[CrossRef](#)]
37. Peykov, V.; Quinn, A.; Ralston, J. Electrowetting: A model for contact-angle saturation. *Colloid Polym. Sci.* **2000**, *278*, 789–793. [[CrossRef](#)]
38. Wu, H.; Hayes, R.; Li, F.; Henzen, A.; Shui, L.; Zhou, G. Influence of fluoropolymer surface wettability on electrowetting display performance. *Displays* **2018**, *53*, 47–53. [[CrossRef](#)]
39. Patel, M.; Kim, S.; Nguyen, T.; Kim, J.; Wong, C. Transparent sustainable energy platform: Closed-loop energy chain of solar-electric-hydrogen by transparent photovoltaics, photo-electro-chemical cells and fuel system. *Nano Energy* **2021**, *90*, 106496. [[CrossRef](#)]
40. Liu, L.; Wu, Z.; Wang, L.; Zhang, T.; Li, W.; Lai, S.; Bai, P. Design of an ac driving waveform based on characteristics of electrowetting stability for electrowetting displays. *Front. Phys.* **2020**, *8*, 618752. [[CrossRef](#)]
41. Patel, M.; Seo, J.H.; Nguyen, T.T.; Kim, J. Active energy-controlling windows incorporating transparent photovoltaics and an integrated transparent heater. *Cell Rep. Phys. Sci.* **2021**, *2*, 100591. [[CrossRef](#)]
42. Mugele, F.; Baret, J.-C. Electrowetting: From basics to applications. *J. Phys. Condens. Matter* **2005**, *17*, R705. [[CrossRef](#)]

Disclaimer/Publisher's Note: The statements, opinions and data contained in all publications are solely those of the individual author(s) and contributor(s) and not of MDPI and/or the editor(s). MDPI and/or the editor(s) disclaim responsibility for any injury to people or property resulting from any ideas, methods, instructions or products referred to in the content.